AIAA'88

AIAA-88-3138

Particle-Laden Weakly Swirling Free Jets: Measurements and Predictions

Daniel L. Bulzan, NASA Lewis Research Center, Cleveland, OH; Jian-Shun Shuen, Sverdrup Technology, Inc., (Lewis Research Center Group), NASA Lewis Research Center, Cleveland, OH; and Gerard M. Faeth, The University of Michigan, Ann Arbor, MI

AIAA/ASME/SAE/ASEE 24th JOINT PROPULSION CONFERENCE

JULY 11-13, 1988/Boston, Massachusetts

PARTICLE-LADEN WEAKLY SWIRLING FREE JETS: MEASUREMENTS AND PREDICTIONS

Daniel L. Bulzan
NASA Lewis Research Center
Cleveland, Ohio 44135

Jian-Shun Shuen*
Sverdrup Technology, Inc.
(Lewis Research Center Group)
NASA Lewis Research Cneter
Cleveland, Ohio 44135

and

Gerard M. Faeth**
The University of Michigan
Ann Arbor, Michigan 48109

E-4176

Abstract

A theoretical and experimental investigation of particle-laden, weakly swirling, turbulent free jets was conducted. Glass particles, having a Sauter mean diameter of 39 μm with a standard deviation of 15 μm, were used in the study. A single loading ratio (the mass flow rate of particles per unit mass flow rate of air) of 0.2 was used in the experiments. Measurements are reported for three swirl numbers, ranging from 0 to 0.3. The measurements included mean and fluctuating velocities of both phases, and particle mass flux distributions. Measurements were compared with predictions from three types of multiphase flow analysis, as follows: (1) locally homogeneous flow (LHF), where slip between the phases was neglected; (2) deterministic separated flow (DSF), where slip was considered but effects of turbulence/particle interactions were neglected; and (3) stochastic separated flow (SSF), where effects of both interphase slip and turbulence/particle interactions were considered using random sampling for turbulence properties in conjunction with random-walk computations for particle motion. For the particle-laden jets, the LHF and DSF models did not provide very satisfactory predictions. The LHF model generally overestimated the rate of decay of particle mean axial and angular velocities with streamwise distance, due to the neglect of particle inertia. LHF model predictions of particle mass flux also showed poor agreement with measurements due to the assumption of no-slip between phases. The DSF model also performed quite poorly for predictions of particle mass flux, because turbulent dispersion of the particles was neglected. The SSF model, which accounts for both particle inertia and turbulent dispersion of the particles, yielded reasonably good predictions throughout the flow field for the particle-laden jets.

Nomenclature

a	acceleration of gravity
C_D	drag coefficient
C_i	parameters in turbulence model
d	injector diameter
d_p	particle diameter
f	mixture fraction
G	particle mass flux
k	turbulence kinetic energy
L_e	dissipation length scale of eddy
m_p	particle mass
n	number of particle groups
$\dot{n}_i$	number of particles per unit time in group i
p	pressure
R	injection tube radius
Re	Reynolds number
r	radial distance
S_ϕ	source term
$S_{p\phi}$	source term due to particles
t	time
t_e	eddy lifetime
u	axial velocity
V_j	volume of computational cell j
v	radial velocity
w	angular velocity
x	axial distance
$\vec{x}_p$	particle position vector
Δx_p	relative path length of particles in an eddy
Δt_p	particle residence time in an eddy

*Senior research engineer; member AIAA.
**A.B. Modine Professor of Aerospace Engineering; fellow AIAA.

ε rate of dissipation of turbulence kinetic energy

μ_t turbulent viscosity

ρ density

σ_i turbulent Prandtl/Schmidt number

ϕ generic property

Subscripts:

c centerline quantity

m maximum value

o injector exit condition

p particle property

∞ ambient condition

Superscripts:

( )' root-mean-square fluctuating quantity

$(\bar{})$ time averaged value

$(\vec{})$ vector quantity

$(\tilde{})$ Favre averaged value

Introduction

Multiphase flows are extremely important in many practical devices. In a gas turbine engine, for example, fuel is sprayed into a highly turbulent recirculating flowfield, where it evaporates and takes part in chemical reactions. Particle-laden flows are being studied as a step toward a better understanding of complex multiphase flows. Particle-laden flows allow the study of interactions between the continuous and dispersed phases without interference from vaporization or combustion effects. The objective of the present investigation was to extend previous work on free particle-laden jets to consider effects of swirl, which is an important aspect of many practical sprays. The performance of typical two-phase flow models was of particular interest. Earlier theoretical and experimental investigations of particle-laden jets have recently been reviewed;[1] therefore, the present discussion of past work will be brief.

Earlier investigations involving analysis and experiments for nonswirling particle-laden jets are reported in Refs. 2 to 5. A recent study of nonswirling particle-laden jets is reported by Mostafa, et al.[6] Three methods of analyzing multiphase flows were considered in these studies, as follows: (1) a locally homogeneous flow (LHF) model, where properties of both phases were taken to be the same; (2) a deterministic separated flow (DSF) model, where finite interphase transport was considered but effects of turbulence on particle motion were ignored; and (3) a stochastic separated flow (SSF) model, where effects of both finite interphase transport rates and turbulence on particle motion were considered using random sampling techniques. In general, the LHF and DSF models over- and under-estimated rates of particle spread and flow development, respectively. In contrast, the SSF model yielded encouraging predictions of flow structure--except at high particle mass loadings, where effects of particles on turbulence proper- ties (termed turbulence modulation by AlTaweel and Landau[7]) which were not considered in the theory, were felt to be responsible for the deficiency.

Relatively few theoretical studies treating particle-laden swirling flows have been published. Hamed[8] modeled the trajectories of solid particles in a flow downstream of swirler vanes. Dring and Suo[9] calculated particle trajectories in a free-vortex flow. Effects of turbulence on particle trajectories, however, were not considered in either of these studies.

Due to the absence of existing measurements, the present experimental study was conducted to obtain data that could be used to assess multiphase flow models in a swirling flowfield. In order to obtain significant interaction between phases, relatively small particles (SMD = 39 μm) were used. Emphasis was placed on obtaining gas-phase velocities in the presence of particles without signal interference from particles. Initial conditions were measured near the jet exit. Single-phase jets were also studied to establish baseline results and are reported in Ref. 10. Also reported in Ref. 10 are predictions of particle-laden swirling jets based on a single particle size, the SMD.

The present paper presents additional measurements and predictions for particle-laden swirling jets. Predictions are reported for the separated-flow models using seven particle size groups in order to better simulate the size distribution of the particles that were used in the study. Predictions from the LHF model are not dependent on particle size; therefore, predictions from the LHF model reported in the present paper are identical to those in Ref. 10.

Experimental Methods

Test Apparatus

The particle-laden jets were directed vertically downward within a large enclosure (1.8 m^2 by 2.4 m high) screened enclosure. The injector could be traversed vertically within the enclosure while the enclosure and injector could be traversed together in the two horizontal directions. This arrangement allowed rigid mounting of all optical instrumentation used during the study.

The jet tube had an inside diameter of 19 mm and extended vertically downward for 100 injector diameters. Swirl was generated by injecting air tangentially through four 9.5 mm long slots, located 481.0 mm upstream of the jet exit. The swirl number (calculated as in Ref. 10) was changed by varying the amount of air injected through the tangential slots. Both the swirl and main air streams were metered with calibrated, critical-flow orifices. The solid-glass particles used during the study were injected into the flow far upstream of the injection tube using a vibrating, variable-speed screw feeder. The size distribution of the particles used in the study is illustrated in Fig. 1. Particle size generally ranged

from about 10 to 65 μm. Test conditions for the present study are summarized in Table I. Three particle-laden jets were studied with swirl numbers ranging from 0 to 0.3. A single loading ratio of 0.2 was considered.

Instrumentation

Gas velocity. Gas-phase velocities were measured in the presence of particles using a single-component phase/Doppler particle analyzer, described in detail by Bachalo and Houser.[11,12] With this instrument, particle size and velocity were measured simultaneously. Gas-phase velocity was measured by seeding the particle-laden jet and ambient surroundings with 1 μm nominal aluminum oxide particles and using the velocity measured for this size to represent the continuous phase. The green (514.5 nm) line of an Ar-Ion laser was used with a 602.4 mm focal-length lens. To reduce the size of the probe volume, a beam expansion ratio of 3 was used. The receiving optics were mounted 30° off-axis in the forward scatter direction, with light collected using a 495 mm focal-length lens. Since frequency shifting was not available for this system; measurements of radial and angular velocities were not performed, and only mean and fluctuating axial velocities are reported.

Particle velocity. Particle velocity was measured using two instruments. Particle velocities, number averaged over all particle sizes, were measured using a two-channel (frequency-shifting on both channels) Ar-Ion laser velocimetry (LV) system. The receiving optics were placed ~30° off-axis in the forward scatter direction. A 602.4 mm focal-length lens was used to collect the scattered light. Seeding particles were not introduced into the flow during the particle velocity measurements and both laser power and detector gain were reduced to insure that only signals from test particles were received. At each axial position, two traverses, 90° degrees apart yielded all required velocity components.

Particle axial velocities were also measured using the phase/Doppler particle analyzer that was used to measure gas-phase velocities. For the particle velocity measurements, laser power was reduced to minimize signals from seeding material and to maximize signals from the particles. Mean and fluctuating axial velocities for particles ranging in size from 3.4 to 94.3 μm were measured.

Particle mass flux. Particle mass flux was measured using an isokinetic sampling probe. Samples were collected on filter paper for a timed interval and weighed. Probes having inside diameters of 2 and 5 mm were used to insure adequate resolution and reasonable sampling times in various regimes of the flow. Measured particle mass fluxes integrated across the jet were within ±10 percent of the calibrated particle flow rate at all axial locations.

Theoretical Methods

General Description

The analysis is limited to steady, axisymmetric, dilute, solid-particle-laden, weakly swirling turbulent jets in an infinite stagnant medium. The swirl number is restricted to values less than ~0.5 to prevent any zones of recirculation. The boundary-layer approximations are adopted, however, the radial pressure gradient, which is usually neglected in the boundary-layer analysis, is considered. A k-ε turbulence model is used to provide closure. The injector Mach number is <0.3; therefore, the kinetic energy and viscous dissipation of the mean flow are neglected with little error.

Three methods of treating multiphase flow, typical of current practice, are considered. The methods are: (1) locally homogeneous flow (LHF), where interphase transport rates are assumed to be infinitely fast and the flow can be treated like a single-phase, variable-density fluid; (2) deterministic separated flow (DSF), where finite interphase transport rates are considered but the dispersed phase is assumed to interact only with mean properties of the continuous phase; and (3) stochastic separated flow (SSF), where interphase transport rates and effects of turbulent dispersion of the dispersed phase are treated. All three methods will be only briefly discussed since they have been fully described elsewhere.[1-6]

Continuous Phase

Mean quantities for the continuous phase are found by solution of governing equations for conservation of mass and momentum in conjunction with second-order turbulence model equations for turbulent kinetic energy and its rate of dissipation. The volume fraction of the particle phase was neglected, since void fractions (volume fraction of flow without particles) for the present flows exceeded 99.8 percent. The governing equations for the continuous phase can be put into the following general form:

$$\frac{\partial}{\partial x}\left(\bar{\rho}\tilde{u}\tilde{\phi}\right) + \frac{1}{r}\frac{\partial}{\partial r}\left(r\bar{\rho}\tilde{v}\tilde{\phi}\right) = \frac{1}{r}\frac{\partial}{\partial r}\left\{r\left(\mu + \frac{\mu_t}{\sigma_\phi}\right)\frac{\partial \phi}{\partial r}\right\} + S_\phi \qquad (1)$$

The parameters ϕ, S_ϕ, and $S_{p\phi}$ appearing in Eq. (1), as well as empirical constants, are summarized in Table II.

A consequence of the presence of angular velocity is that even though the standard boundary-layer assumptions have been made, the radial momentum equation still must be considered:

$$\frac{\partial \bar{p}}{\partial r} = \frac{\bar{\rho}\tilde{w}^2}{r} \qquad (2)$$

and cross-stream pressure gradients are not negligible. Due to the decay of angular velocity, the axial pressure gradient is also included.

The turbulent viscosity was calculated as usual:

$$\mu_t = C_\mu \bar{\rho} \bar{k}^2 \Big/ \varepsilon \qquad (3)$$

The flow leaving the injector was similar to fully developed flow and had no potential core. The boundary conditions for Eq. (1) are:

$$\phi \neq r\tilde{w} : r = 0, \frac{\partial \phi}{\partial r} = 0; \; r \to \infty, \phi = 0$$

$$\phi = r\tilde{w} : r = 0, r\tilde{w} = 0; \; r \to \infty, r\tilde{w} = 0 \tag{4}$$

Initial conditions were measured at x/d = 0.5. ε_o was calculated from the definition of a turbulent length scale, as follows:

$$\varepsilon_o = \frac{C_\mu k^{3/2}}{L} \tag{5}$$

where L was chosen as a fraction of the initial jet width to provide good agreement with the axial profile for k. Since only $\bar{u}$ and u' could be measured for the particle-laden cases, initial values of the continuous-phase angular velocity were estimated by subtracting the measured particle angular momentum from the single-phase values. Single-phase initial values of k and ε were used for the particle-laden jet calculations.

The present stochastic separated flow approach involves modification and extension of methods reported by Gosman and Ioannides.[13] This involves computing particle motion as particles interact with a succession of turbulent eddies. Properties are assumed to be uniform within each eddy and to randomly change from one eddy to the next. At the start of a particle-eddy interaction, the velocity of an eddy is found by making a random selection from the probability density function (PDF) of velocity--assuming an isotropic Gaussian PDF having standard deviations $(2k/3)^{1/2}$ and mean values $\bar{u}$, $\bar{v}$, and $\bar{w}$. A particle is assumed to interact with an eddy for a time which is the minimum of either the eddy lifetime or the time required for a particle to cross an eddy. These times are estimated following past practice,[2-5] assuming that the characteristic size of an eddy is the dissipation length scale:

$$L_e = C_\mu^{3/4} k^{3/2}/\varepsilon \tag{6}$$

and that the eddy lifetime is:

$$t_e = L_e/(2k/3)^{1/2} \tag{7}$$

Therefore, particles are assumed to interact with an eddy as long as both the time and distance of interaction satisfy the following criteria:

$$\Delta t_p \leq t_e, \; \Delta \vec{x}_p \leq L_e \tag{8}$$

Assumptions for particle trajectory calculations are typical of analysis of dilute particle-laden flows:[1] drag is treated empirically, assuming quasisteady flow for spherical particles with no influence of nearby particles; particle collisions are neglected; effects of virtual mass, Bassett forces and Magnus forces are neglected with little error, since $\rho_p/\rho > 2000$; and static-pressure gradients are negligible. Local ambient properties are fixed by instantaneous eddy properties, as described earlier, which implicitly provides for effects of turbulent fluctuations on particle dispersion and drag.

With these assumptions, the position and velocity for each particle group can be found by integrating:

$$\frac{dx_{pi}}{dt} = u_{pi} \tag{9}$$

$$\frac{du_{pi}}{dt} = \left(\frac{3\rho C_D}{4 d_p \rho_p}\right)(u_i - u_{pi})\left|\vec{u} - \vec{u}_p\right| + a_i \tag{10}$$

where i = 1,2,3 and the velocities shown in these equations are instantaneous velocities for a particular eddy and particle group. Since the particles are solid spheres, the drag coefficient was calculated as follows:[1]

$$C_D = \frac{24}{Re}\left(1 + \frac{Re^{2/3}}{6}\right), \; Re < 1000;$$

$$C_D = 0.44, \qquad Re > 1000 \tag{11}$$

Dispersed Phase

SSF model. The dispersed phase was treated by solving Lagrangian equations for the trajectories of a statistically significant sample of individual particles (n groups defined by initial position, velocity and sample) as they move away from the injector and encounter a random distribution of turbulent eddies. This approach provides a means of treating effects of turbulent fluctuations on particle drag and dispersion as well as effects of particles on turbulence properties. Predictions presented in the present paper for the SSF model utilized 7000 particle groups.

Key elements of the SSF model are the methods used to specify eddy properties and the time of interaction of a particle with a particular eddy.

Particle source terms. The interaction between particles and the continuous phase yields source terms in the governing equations for conservation of axial and angular momentum. The source terms are found by computing the net change in momentum as each particle group i passes through computational cell j

$$S_{pu_j} = V_j^{-1} \sum_{i=1}^{n} \dot{n}_i m_p \left(u_{pi_{in}} - u_{pi_{out}}\right)_j \tag{12}$$

$$S_{prw_j} = V_j^{-1} \sum_{i=1}^{n} \dot{n}_i m_p \left(\left(rw_{pi}\right)_{in} - \left(rw_{pi}\right)_{out}\right)_j \tag{13}$$

where $\dot{n}_i$ is the number of particles per unit time in each group.

DSF model. Effects of turbulent fluctuations on particle drag and dispersion are ignored for the DSF model. Particle trajectories are found by integrating Eqs. (9) and (10), but the local mean velocity of the continuous phase replaces the instantaneous eddy velocity. Each initial condition yields a single deterministic trajectory; therefore, 1400 particle groups suffice to numerically close the solution. Effects of particle drag in the mean momentum equations are found from Eqs. (12) and (13), similar to the SSF calculations.

LHF model. This approximation implies that both phases have the same instantaneous velocity at each point in the flow; therefore, the flow corresponds to a variable-density, single-phase fluid whose density changes due to changes in particle concentration. Turbulent dispersion of particles is then equivalent to that of a gas and particle inertia fully influences turbulence properties; i.e., the method implicitly accounts for effects of turbulence modulation to the extent that the no-slip assumption is correct.

The treatment of the variable-density fluid is similar to past practice, however $\tilde{f}$ is defined here as the mass fraction of particles in the fluid. Measured initial values of $\tilde{f}$ were used for the LHF predictions. Through the assumption of no-slip, there is no need to compute particle trajectories and all particle source terms in the governing equations for the continuous phase are zero.

Numerical Solution

The calculations for the continuous phase were performed using a modified version of GENMIX.[14] The computational grid for the cases without swirl was similar to past work:[2-5,10] 33 cross-stream grid nodes and streamwise step size was limited to 5 percent of the current flow width or an entrainment increase of 5 percent-whichever was smaller. For the cases with swirl, 33 cross-stream grid nodes were also used, but streamwise step size was reduced to the smaller of either 2 percent of the current flow width or an entrainment increase of 2 percent. The angular and radial momentum equations required modifications to the standard solution procedure and this procedure is described in Ref. 10.

Results and Discussion

Predictions and measurements of the particle-laden jets are discussed in the following. As discussed earlier, only mean and fluctuating axial velocities could be measured for the gas phase; therefore, it was necessary to estimate initial values of angular velocity and turbulent kinetic energy for the gas phase. Initial angular velocity of the continuous phase was estimated by subtracting the measured initial particle-phase angular momentum from the values obtained for single-phase cases. For both swirl flows, particle-phase angular momentum was ~10 percent of the values measured for the single-phase cases. For the predictions shown here, initial values of k were assumed to be the same as the single-phase flows. Measured values of u' were ~20 percent lower across the entire jet width for the particle-laden cases (at the initial condition of $x/d = 0.5$) than for the corresponding single-phase flows. Predictions showed that a reduction of k of 20 percent caused negligible changes in flow properties except very close to the injector. Initial values of ε for the particle-laden jet predictions were also unchanged from the single-phase cases.

For the separated-flow models, the predictions utilized seven particle size groups ranging in size from 12.5 to 72.5 μm. Initial axial mean and fluctuating velocities for each particle size group were obtained from phase/Doppler measurements at $x/d = 0.5$. Initial mean and fluctuating angular and radial velocities were obtained from LV measurements at $x/d = 0.5$; thus each size group was given the same initial angular and radial velocity.

For the LHF model, predictions are not dependent on particle size; therefore, predictions presented in the present paper are identical to those reported in Ref. 10.

Nonswirling Jet

The predicted and measured variation of axial velocities in the streamwise direction for the nonswirling, particle-laden jet are illustrated in Fig. 2. Measured particle velocities reported in Fig. 2(b) are number averaged over all particle sizes. For comparison with these measurements, predictions from the separated-flow models were number averaged over all seven size groups as well. Because the particle loading ratio is relatively low, predictions from both the LHF and SSF models are nearly identical and show reasonably good agreement with the experimental measurements. For the gas-phase axial velocity, deterministic separated flow model predictions were identical to those from the stochastic separated flow model and are not shown. Particle axial velocity predictions (Fig. 2(b)) using the LHF model and separated-flow models show distinct differences. The neglect of particle inertia, illustrated by predictions from the LHF model, overestimates the rate of decay of particle axial velocity. Predictions from both the stochastic and deterministic models are similar and show reasonably good agreement with measurements for particle axial velocity decay.

Radial profiles of flow properties, number averaged over all particle sizes, for the particle-laden jets without swirl are illustrated in Figs. 3 and 4. Measurements and predictions are illustrated for $x/d = 5$ and 30. Gas-phase jet widths are slightly overestimated for the particle-laden flows at $x/d = 30$ (Fig. 4). The overestimation of gas-phase flow width is probably caused by turbulence modulation due to the particles. Even though the loading ratio was relatively low, values of u' for the particle-laden jets are reduced compared to the single-phase jets.[10] Particle axial velocities are reasonably well predicted by all the models, however, since the LHF model overestimates the rate of axial velocity decay with streamwise distance, the values of axial velocity predicted by this approach are generally lower than the measurements.

Radial profiles of particle mass flux (Figs. 3(c) and 4(c)) illustrate the different physical assumptions embodied in the three models. At $x/d = 5$, both separated flow models give similar predictions of particle mass flux. At larger streamwise distances, however, the neglect of turbulent dispersion of the particles causes the DSF model to underestimate the spread of the particles. Since mean gas-phase radial velocities are quite small at these axial distances, turbulent dispersion is the only mechanism available for radial spread of the particles. The no-slip assumption of the LHF model causes the radial dispersion of the particles to be overestimated at $x/d = 30$. Only the SSF model, which accounts for both particle inertia and turbulent dispersion of the

particles, satisfactorily predicts the radial particle mass flux at x/d = 30.

The predictions of fluctuating particle properties for the SSF model, also illustrated in Figs. 3(a) and 4(a), are reasonably good, however, u'_p is underestimated. This is probably caused by the assumption of isotropic velocity fluctuations, which causes streamwise continuous-phase velocity changes experienced by the particle to be underestimated. In particular, measured values of u' are always greater than v' and w' for the single-phase jet[10] and it is expected that this behavior should be similar for the particle-laden jet. For the nonswirling jet, predictions using seven size groups are almost identical to those previously reported[10] using the SMD of the particle distribution.

These results for the particle-laden jets without swirl are similar to those previously reported by other investigators for similar flows.[1-6]

Measurements and predictions of particle mean axial velocity for 23, 43, and 63 μm particles at x/d = 5, 15, and 30 are illustrated in Fig. 5 for the nonswirling jet. The data presented were obtained using the phase/Doppler particle analyzer and represent axial velocities of particles from the size distribution shown in Fig. 1. Only predictions from SSF model are presented. As illustrated in Fig. 5, decay of axial velocity of the larger particles is slower than the smaller particles. By x/d ≈ 15, the 63 μm particles have the highest velocity. Predictions from the SSF model are in reasonably good agreement with measurements and correctly show the general trends.

Swirling Jets

Measurements and predictions for the particle-laden swirling jets are discussed in this section. Jets having swirl numbers of S = 0.16 and 0.3 were studied.

Predicted and measured flow properties in the streamwise direction are illustrated in Figs. 6 to 8 for the swirling, particle-laden jets. Predicted and measured gas-phase axial velocities are shown in Fig. 6 for swirl numbers of 0.16 and 0.3. As illustrated in Fig. 6, increasing swirl increases the rate of decay of axial velocity. Predictions from the LHF and SSF models are nearly identical and show reasonably good agreement with measurements for both swirling flows. Again, predictions of gas-phase axial velocity using the DSF model are nearly identical to predictions using the SSF model and are not shown in the figure.

Particle mean axial and maximum angular velocities, number averaged over all particle sizes, are plotted as a function of streamwise distance in Figs. 7 and 8, respectively. As expected, neglecting slip between the phases causes predictions from the LHF model to overestimate the rate of decay of particle velocities. Differences between predictions from the DSF and SSF models were small: both show reasonably good agreement with measurements. At the initial condition (x/d = 0.5), axial velocities of the particles were lower than the continuous phase except near the edge of the jet for both swirling flows. Particle axial velocities initially increase, due to momentum exchange from the continuous phase, before beginning to decay. As illustrated in Fig. 7, both separated-flow models correctly predict this behavior.

Radial profiles of flow properties for the particle-laden swirling jets are illustrated in Figs. 9 to 14. Velocity measurements, number averaged over all particle sizes, are illustrated in Figs. 9 to 12. Particle mean axial velocities for three size groups are illustrated in Figs. 13 and 14 for the two swirling flows.

Radial profiles of number-averaged flow properties for the swirling, particle-laden jets at x/d = 5 are illustrated in Figs. 9 and 10 for S = 0.16 and 0.3 ,respectively. As expected, increasing the swirl number increases the width of the particle-laden jet. The gas-phase flow width is slightly overestimated at x/d = 5 for both swirling flows. Again, this is probably due to turbulence modulation by the particles, as discussed earlier. Also, because the gas-phase flow width is overestimated, particle axial velocities are also overestimated for the separated-flow models. The SSF model overestimates particle axial velocity to a greater extent than the DSF model. The LHF model, however, underestimates particle axial velocity, due to the neglect of particle inertia. At x/d = 5, particle axial velocity, number averaged over all size groups, is nearly equal to the continuous phase. For both swirling flows, the LHF model predicts that the maximum particle mass flux has shifted to the center of the jet, which is clearly not correct. The neglect of turbulent dispersion of the particles, illustrated by the DSF model, causes the particles to be confined to a relatively narrow region of the flow. If only mean properties of the continuous phase are considered, the particles are transported by centrifugal forces to regions where radial velocity is small and tend to remain there. Considering turbulent fluctuations of the continuous phase gives better predictions of particle mass flus at x/d = 5. The predicted maximum particle mass flux is shifted radially outward when compared to the measurements. This is again probably caused by the overestimation of the jet width at this streamwise location. Predictions of mean particle angular and fluctuating velocities are quite good for the S = 0.16 flow, see Fig. 9(e). For the higher swirl number flow, S = 0.3, particle fluctuating axial velocities are overestimated (see Fig. 10), however, predictions of the other two fluctuating particle velocities show better agreement with measurements. Predicted particle fluctuating velocities are increased at all locations using seven particle sizes when compared to predictions using the particle SMD,[10] especially for the higher swirl number flow. Predicted mean properties using the particle SMD are similar to those obtained during the present study using seven particle sizes.

Radial profiles of gas-phase properties at x/d = 20 are illustrated in Figs. 11 and 12 for both swirl flows. Predictions are in better agreement with measurements at this position than closer to the injector, although the jet width is still slightly overestimated. Predictions at

x/d = 20 are not as sensitive to initial conditions and the swirl component has almost completely decayed. Again, there is little difference between predictions of gas-phase properties for the no-slip and separated-flow models. Predictions of axial velocity are in good agreement with measurements for all three models. However, since the LHF model overestimates the rate of decay of axial velocity, predicted unnormalized velocities from this model are lower than the measurements. Predicted values of u'_p underestimate the measurements, while v'_p and w'_p are in reasonably good agreement with measurements using the SSF model. Since effects of swirl have decayed at this axial location, ignoring the anisotropy of the continuous phase is the main reason for this behavior. Even at x/d = 20, predicted fluctuating particle velocities using a single particle size, the $SMD,^{10}$ are slightly lower than those of the present study using seven particle sizes.

The particle mass flux predictions (Figs. 11(c) and 12(c)) again highlight the different physical assumptions of the three models. Particle mass flux measurements indicated that between x/d = 5 and x/d = 10, the maximum mass flux shifted to the center of the jet for both swirl cases. Since angular and radial velocities have decayed to relatively small values at this distance, and would tend to move particles outward, the only mechanisms for transport inward are turbulent dispersion and entrainment of ambient air at the edge of the jet. As shown in Figs. 11(c) and 12(c), the predicted maximum particle mass flux from the SSF model has not completely shifted to the center of the jet, however it is clearly evolving in this direction. In contrast, the DSF model predicts a very narrow distribution with no particles at the center of the jet. Compared to the nonswirling case, the LHF model underestimates particle dispersion for both swirling flows at x/d = 20. This behavior is caused by neglecting the radial and angular inertia of the particles which tend to transport them radially.

Measurements and SSF model predictions of mean axial velocities for particle diameters of 23, 43, and 63 μm in the two swirling flows are illustrated in Figs. 13 and 14. Again, measurements reported for each size group were obtained with the phase/Doppler particle analyzer.

Radial profiles of $\bar{u}$ are shown at axial locations of x/d = 2, 5, 10, and 20. At x/d = 2, the velocity of the smaller particles is larger than the larger particles near the center of the jet. Because of their increased inertia, the axial velocity of the larger particles decays at a slower rate than smaller particles, and by x/d = 20, larger particles are moving at a higher velocity than the smaller particles at all radial locations. Increasing swirl increases the variation of velocity with particle size, see Figs. 13 and 14.

SSF model predictions of mean particle axial velocity for each size group show better agreement with measurements as distance from the injector exit increases. At streamwise distances of x/d = 10 and less, radial profiles of axial velocity were overestimated for both swirling flows. As discussed earlier, this is probably due to turbulence modulation since the continuous-phase jet width was also overestimated for these flows.

At x/d = 5, particle velocities are underestimated for both swirling flows (Figs. 13(b) and 14(b)). Since predicted centerline particle velocities were higher for the DSF model at x/d = 5 and 10, this appears to be the result of eddy specification in the stochastic model. This is especially true for the 23 μm particles. Eddies are assumed to travel at the mean gas-phase velocity at their initial radial position in the flowfield. Smaller particles, which have shorter relaxation times, tend to remain in a particular eddy longer than larger particles.

Predictions from the SSF model display the correct trends with respect to variations in particle velocity with size and streamwise distance. Predictions at x/d = 20 exhibit good agreement with measurements for both swirling flows.

Conclusions

Major conclusions concerning the models that were evaluated during this investigation are as follows:

1. Predictions using the SSF model showed reasonable agreement with measurements for the particle-laden jets. In general, the LHF model overestimated the rate of particle velocity decay in the particle-laden jets due to the neglect of particle inertia. For nonswirling jets, the LHF model overestimated particle spreading rates due to the no-slip assumption. For swirling jets, the LHF model underestimated particle spreading rates due to the neglect of particle inertia. The DSF model underestimated particle spreading rates due to the neglect of the effect of turbulent fluctuations on particle motion. Only the SSF model, which accounts for both particle inertia and effects of turbulent fluctuations, correctly predicted particle spreading rates over the entire flowfield.

2. Particle axial fluctuating velocities were generally underestimated at far downstream axial locations. This is probably due to the assumption of isotropic velocity fluctuations in the SSF model, since fluctuating axial velocities are expected to be greater than fluctuating radial or angular velocities.

3. Near the injector exit, jet widths were overestimated with the separated-flow models. This was probably caused by turbulence modulation by the particles, which was not considered in the analysis.

4. Mean axial velocities for each particle size group were reasonably well predicted for the particle-laden jets using the SSF model. Predictions showed the same trends as measurements for particle streamwise axial velocity decay of each size group.

References

1. Faeth, G.M., "Recent Advances in Modeling Particle Transport Properties and Dispersion in Turbulent Flow," ASME-JSME, Thermal Engineering Joint Conference Proceedings, Vol. 2, Y. Mori and W.J. Yang, eds., ASME, New York, 1983, pp. 517-534.

2. Shuen, J.S., Chen, L.D., and Faeth, G.M., "Evaluation of the Stochastic Model of Particle Dispersion in a Turbulent Round Jet," AICHE Journal, Vol. 29, No. 1, Jan. 1983, pp. 167-170.

3. Shuen, J.S., Chen, L.D., and Faeth, G.M., "Predictions of the Structure of Turbulent, Particle-Laden Round Jets," AIAA Journal, Vol. 21, No. 11, Nov. 1983, pp. 1483-1484.

4. Shuen, J.S., Solomon, A.S.P., Zhang, Q.F., and Faeth, G.M., "Structure of Particle-Laden Jets: Measurements and Predictions," AIAA Journal, Vol. 23, No. 3, Mar. 1985, pp. 396-404.

5. Zhang, Q.F., Shuen, J.S., Solomon, A.S.P., and Faeth, G.M., "Structure of Ducted Particle-Laden Jets," AIAA Journal, Vol. 23, No. 7, July 1985, pp. 1123-1125.

6. Mostafa, A.A., Mongia, H.C., McDonell, V.G., and Samuelson, G.S., "On the Evolution of Particle-Laden Jet Flows: A Theoretical and Experimental Study," AIAA Paper 87-2181, June 1987.

7. Al Taweel, A.M., and Lanadau, J., "Turbulence Modulation in Two-Phase Jets," International Journal of Multiphase Flow, Vol. 3, No. 4, June 1977, pp. 341-351.

8. Hamed, A., "Particle Dynamics of Inlet Flow Fields with Swirling Vanes," AIAA Paper 81-0001, Jan. 1981.

9. Dring, R.P., and Suo, M., "Particle Trajectories in Swirling Flows," Journal of Energy, Vol. 2, No. 4, July-Aug. 1978, pp. 232-237.

10. Buizan, O.L., Shuen, J.S., and Faeth, G.M., "Particle-Laden Swirling Free Jets: Measurements and Predictions," AIAA Paper 87-0303, Jan. 1987. (NASA TM-88904).

11. Bachalo, W.D., and Houser, M.J., "Development of the Phase/Doppler Spray Analyzer for Liquid Drop Size and Velocity Characterizations," AIAA Paper 84-1199, June 1984.

12. Houser, M.J., and Bachalo, W.D., "Extension of the Phase/Doppler Particle Analyzer to Submicron Particle Measurements," Particle Sizing and Spray Analysis, SPIE Proc. Vol. 573, N. Chigier and G.W. Stewart, eds., SPIE, Bellingham, WA, 1985, pp. 57-66.

13. Gosman, A.D., and Ioannides, E., "Aspects of Computer Simulation of Liquid-Fueled Combustors," Journal of Energy, Vol. 7, No. 6, Nov.-Dec. 1983, pp. 482-490.

14. Spalding, D.B., GENMIX: A General Computer Program for Two-Dimensional Parabolic Phenomena, Pergamon Press, Oxford, 1978.

TABLE I. - SUMMARY OF TEST CONDITIONS[a]

Parameter	Case 1	Case 2	Case 3
Centerline air axial velocity, m/s[b]	13.75	11.9	12.2
Maximum air angular velocity, m/s[c]	0	2.84	5.33
Swirl number	0	0.16	0.3
Centerline particle axial velocity, m/s[b]	13.8	10.39	10.26
Maximum particle angular velocity, m/s[b]	0	1.48	2.26
SMD, μm[d]	39	39	39
Loading ratio[e]	0.2	0.2	0.2

[a]Ambient temperature and pressure, 296 K, 97 kPa; injector inside diameter, 19 mm; particle density, 2500 kg/m^3.
[b]Measured at x/d = 0.5.
[c]Estimated from single-phase cases.
[d]The size distribution has a standard deviation of 15 μm.
[e]Ratio of injected particle mass flow rate to air mass flow rate.

TABLE II. - SOURCE TERMS IN GOVERNING EQUATIONS

ϕ	S_ϕ
1	0
$\tilde{u}$	$-\frac{\partial \bar{p}}{\partial x}$
$r\tilde{w}$	$-\frac{1}{r}\frac{\partial}{\partial r}\left\{\left(\mu + \mu_t\right) 2r\tilde{w}\right\}$
$\tilde{f}$	0
k	$\mu_t\left\{\left(\frac{\partial \tilde{u}}{\partial r}\right)^2 + \left[r\frac{\partial}{\partial r}\left(\frac{\tilde{w}}{r}\right)\right]^2\right\} - \bar{\rho}\varepsilon$
ε	$C_{\varepsilon 1}\mu_t\frac{\varepsilon}{k}\left\{\left(\frac{\partial \tilde{u}}{\partial r}\right)^2 + \left[r\frac{\partial}{\partial r}\left(\frac{\tilde{w}}{r}\right)\right]^2\right\} - C_{\varepsilon 2}\bar{\rho}\frac{\varepsilon^2}{k}$

C_μ	$C_{\varepsilon 1}$	$C_{\varepsilon 2}$	σ_k	σ_ε	σ_f
0.09	1.44	1.87	1.0	1.3	0.7

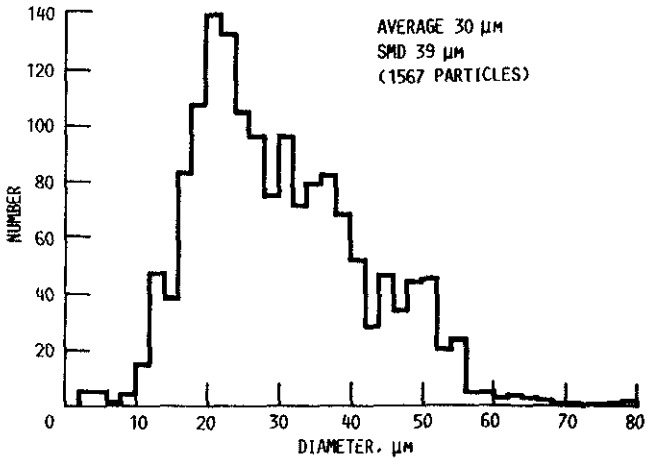

FIGURE 1. - PARTICLE SIZE DISTRIBUTION.

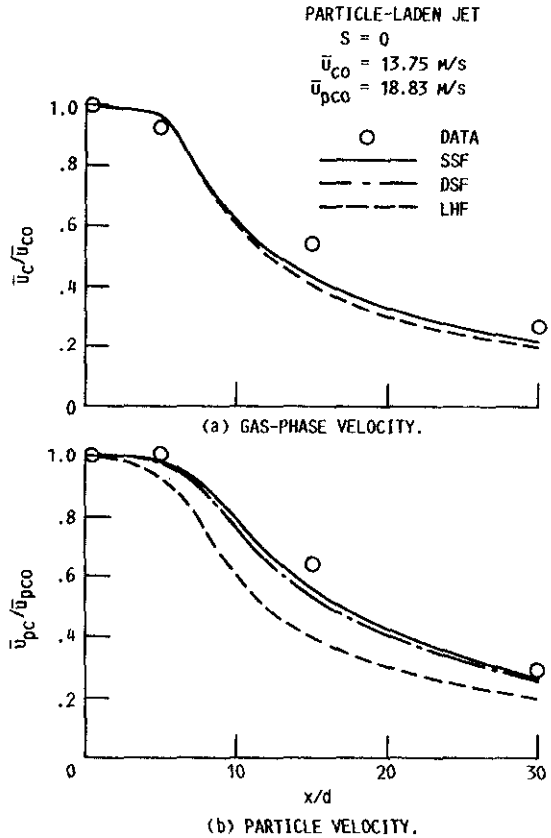

(a) GAS-PHASE VELOCITY.

(b) PARTICLE VELOCITY.

FIGURE 2. - STREAMWISE VARIATION OF NUMBER-AVERAGED AXIAL VELOCITY FOR THE PARTICLE-LADEN JET (S = 0).

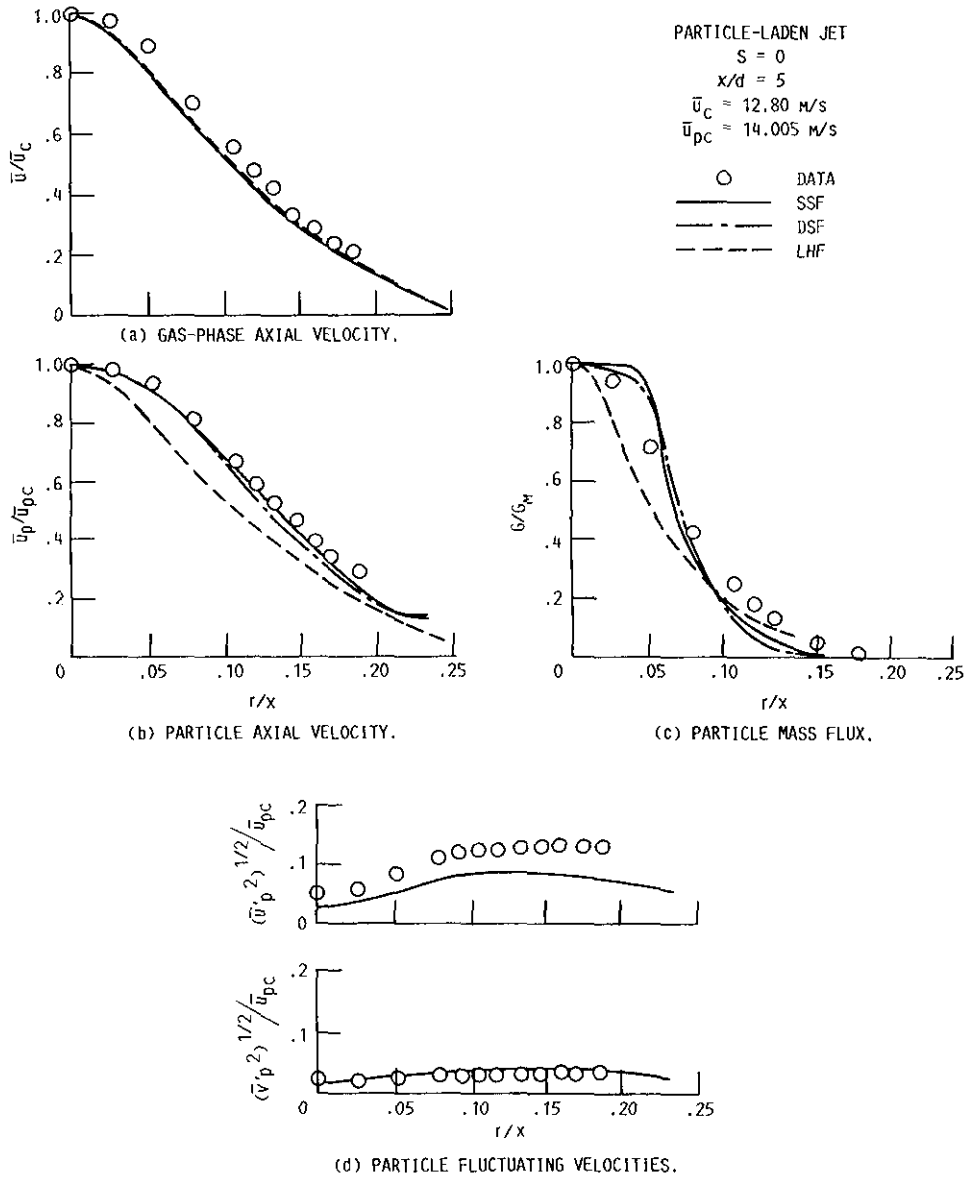

(a) GAS-PHASE AXIAL VELOCITY.

(b) PARTICLE AXIAL VELOCITY.

(c) PARTICLE MASS FLUX.

(d) PARTICLE FLUCTUATING VELOCITIES.

FIGURE 3. - RADIAL VARIATION OF NUMBER-AVERAGED FLOW PROPERTIES AT x/d = 5 FOR THE PARTICLE-LADEN JET (S = 0).

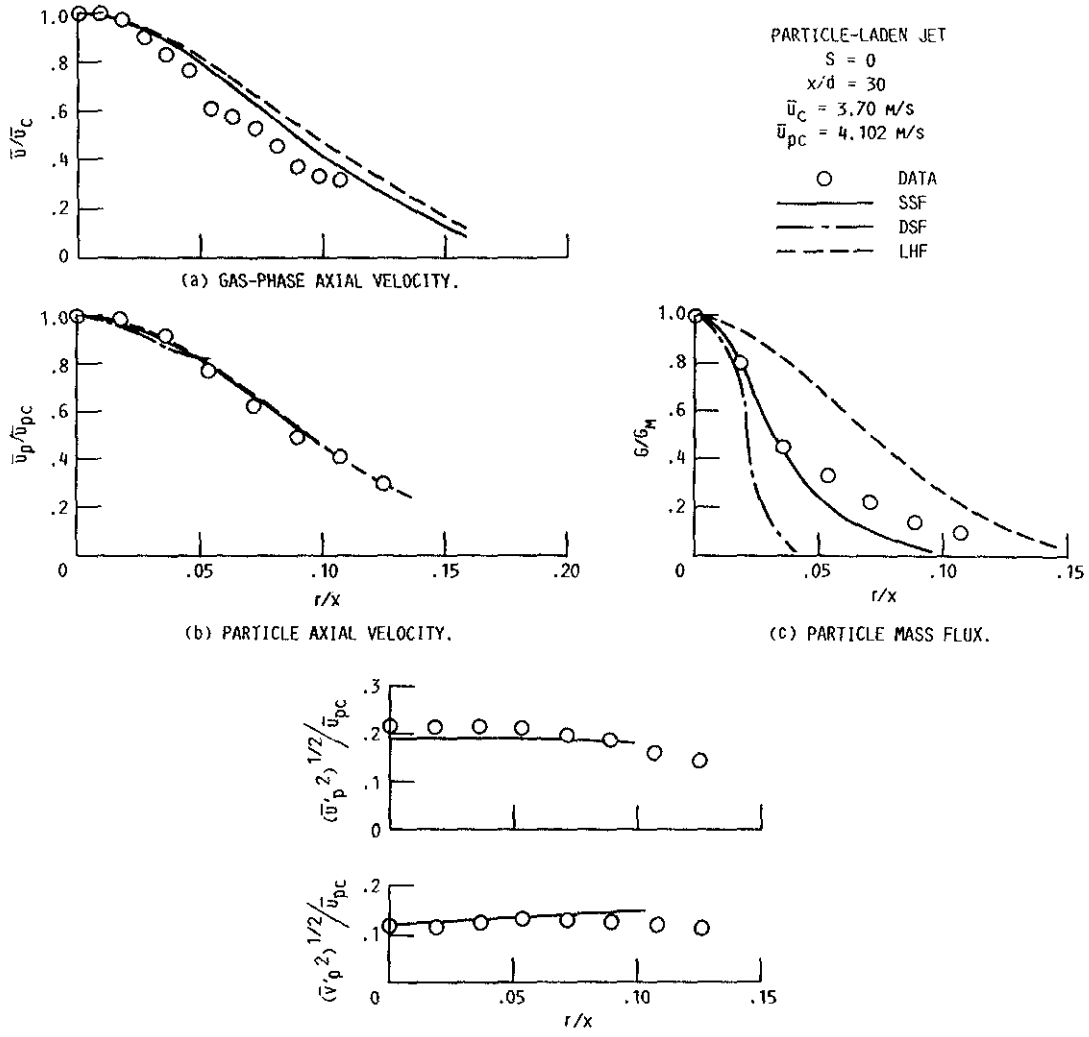

(a) GAS-PHASE AXIAL VELOCITY.

(b) PARTICLE AXIAL VELOCITY.

(c) PARTICLE MASS FLUX.

(d) PARTICLE FLUCTUATING VELOCITIES.

FIGURE 4. - RADIAL VARIATION OF NUMBER-AVERAGED FLOW PROPERTIES AT x/d = 30 FOR THE PARTICLE-LADEN JET (S = 0).

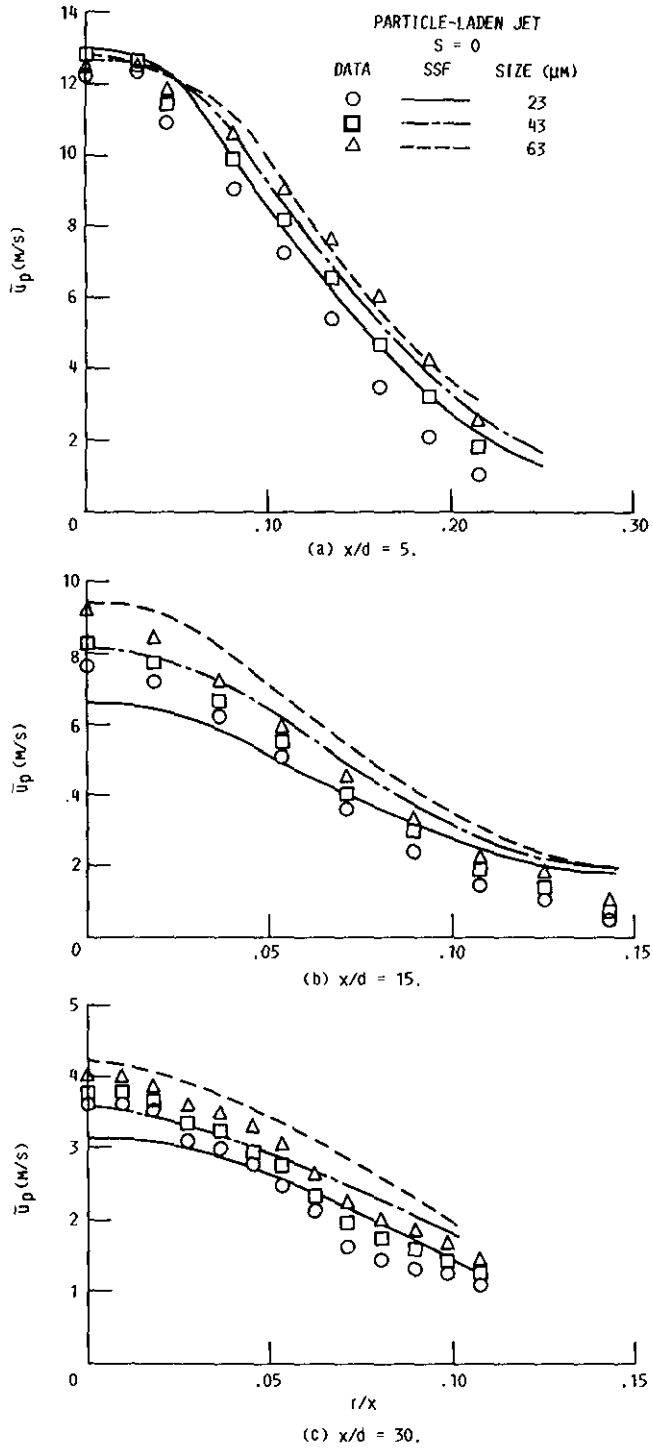

FIGURE 5. - RADIAL VARIATION OF MEAN AXIAL VELOCITY OF 23, 43, AND 63 MICRON PARTICLES AT x/d = 5, 15, AND 30 (S = 0).

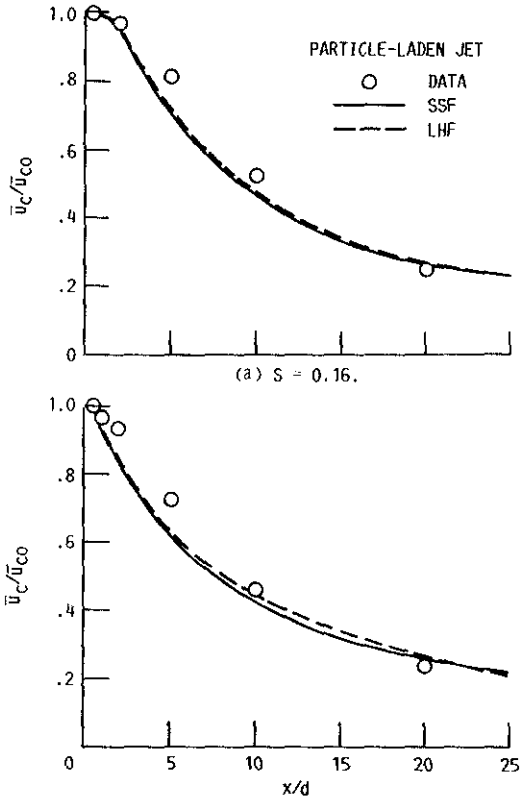

(a) S = 0.16.

(b) S = 0.3.

FIGURE 6. - STREAMWISE VARIATION OF GAS-PHASE AXIAL VELOCITY FOR THE PARTICLE-LADEN SWIRLING JETS.

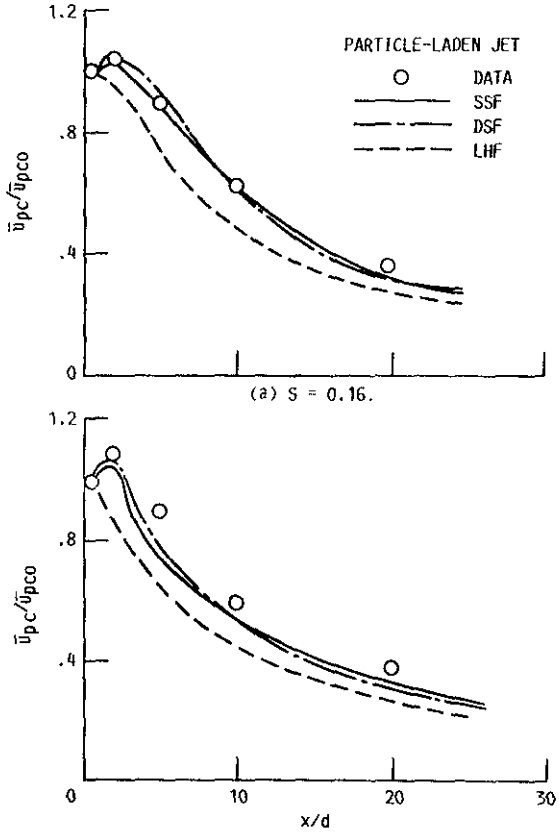

(a) S = 0.16.

(b) S = 0.3.

FIGURE 7. - STREAMWISE VARIATION OF NUMBER-AVERAGED PARTICLE AXIAL VELOCITY FOR THE PARTICLE-LADEN SWIRLING JETS.

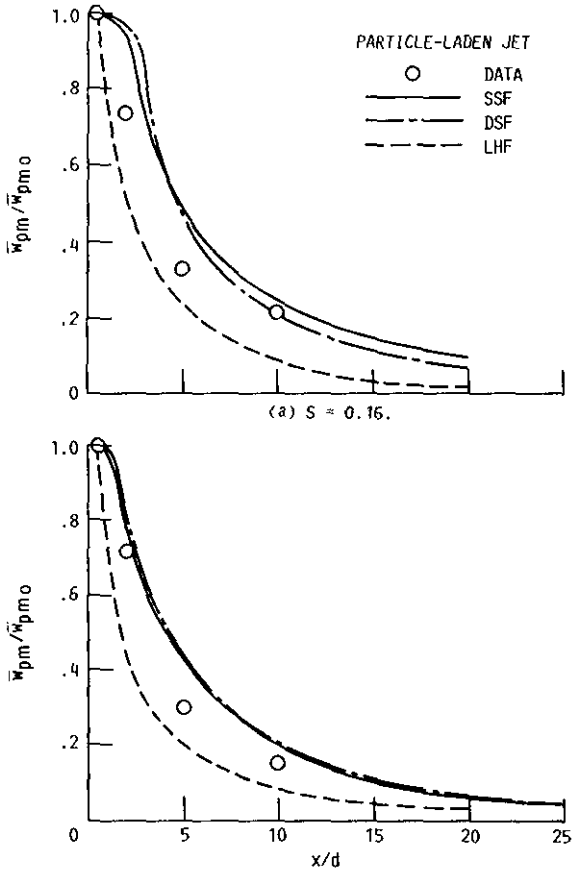

(a) S = 0.16.

(b) S = 0.3.

FIGURE 8. - STREAMWISE VARIATION OF NUMBER-AVERAGED PARTICLE MAXIMUM ANGULAR VELOCITY FOR THE PARTICLE-LADEN SWIRLING JETS.

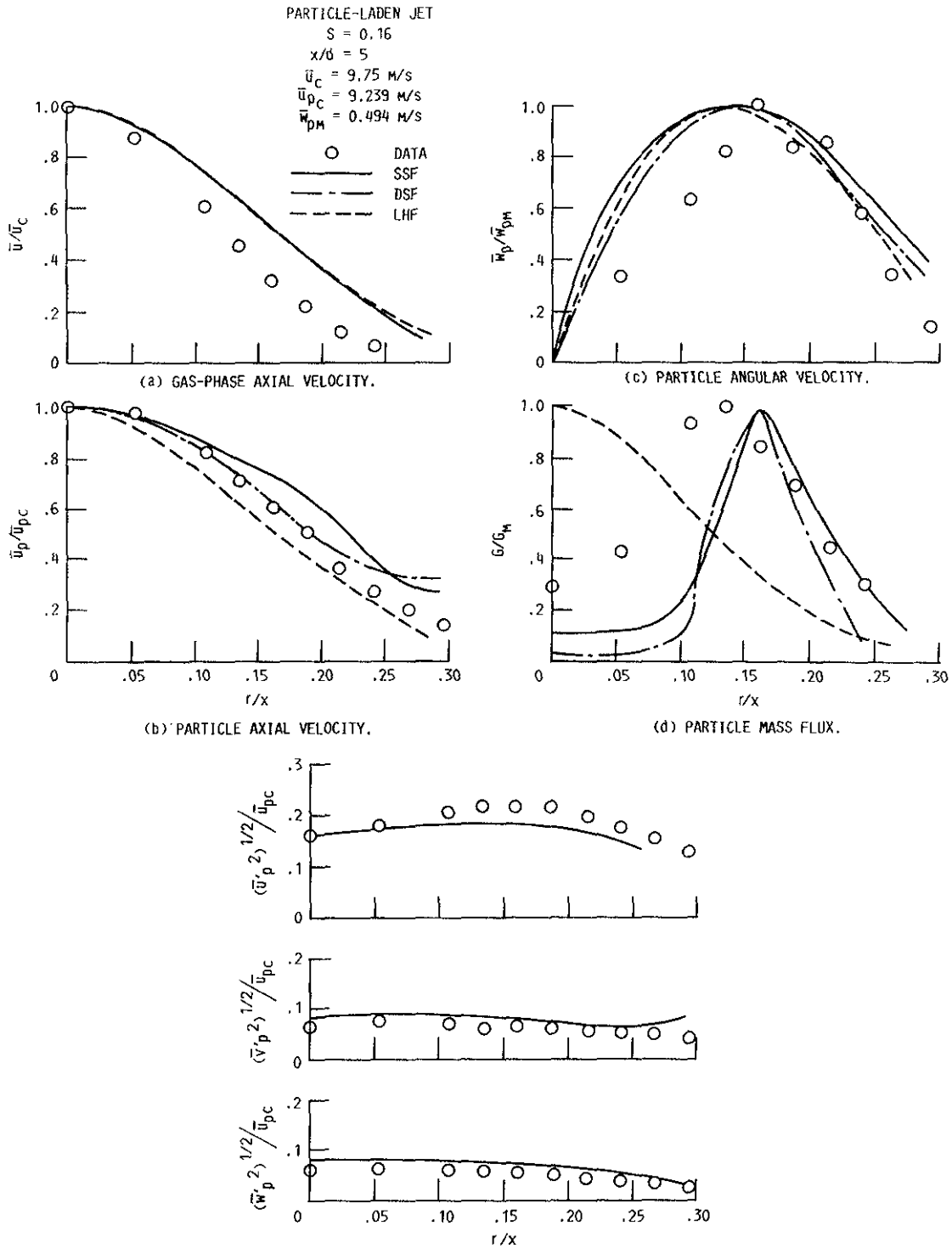

(a) GAS-PHASE AXIAL VELOCITY.

(b) PARTICLE AXIAL VELOCITY.

(c) PARTICLE ANGULAR VELOCITY.

(d) PARTICLE MASS FLUX.

(e) PARTICLE FLUCTUATING VELOCITIES.

FIGURE 9. - RADIAL VARIATION OF NUMBER-AVERAGED FLOW PROPERTIES FOR THE SWIRLING (S = 0.16) PARTICLE-LADEN JET AT x/d = 5.

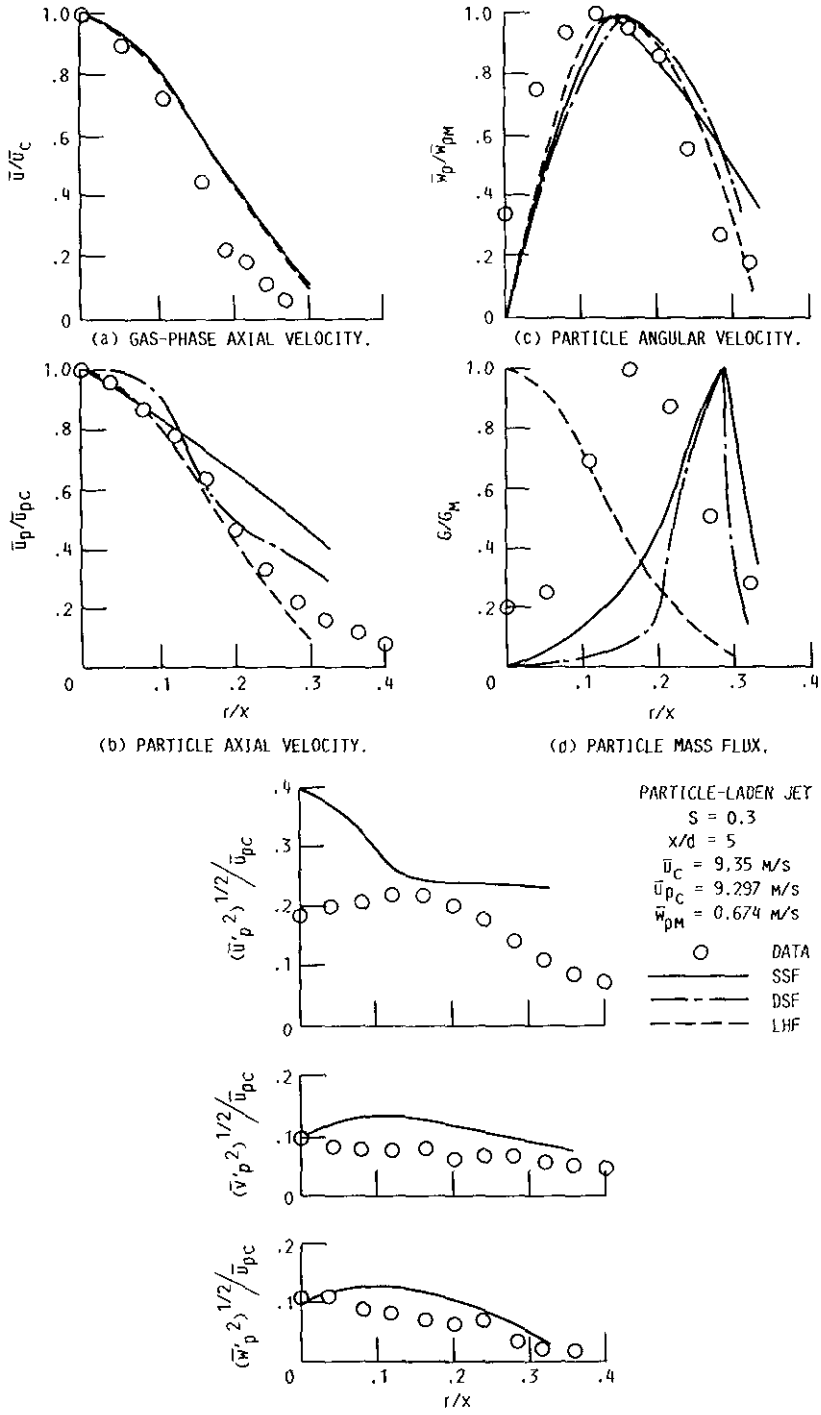

FIGURE 10. - RADIAL VARIATION OF NUMBER-AVERAGED FLOW PROPERTIES FOR THE SWIRLING (S = 0.3) PARTICLE-LADEN JET AT x/d = 5.

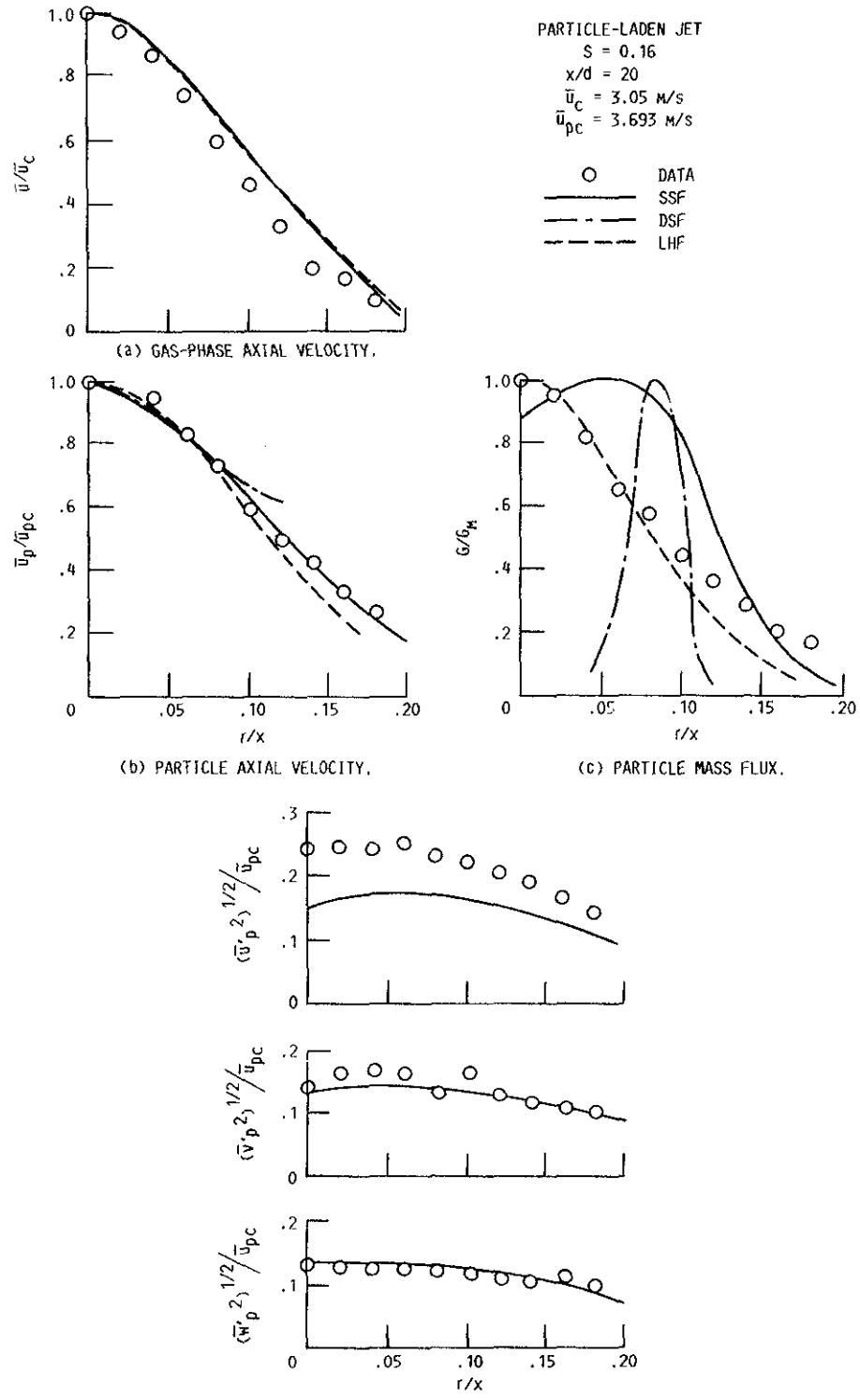

(a) GAS-PHASE AXIAL VELOCITY.

(b) PARTICLE AXIAL VELOCITY.

(c) PARTICLE MASS FLUX.

(d) PARTICLE FLUCTUATING VELOCITIES.

FIGURE 11. - RADIAL VARIATION OF NUMBER-AVERAGED FLOW PROPERTIES FOR THE SWIRLING (S = 0.16) PARTICLE-LADEN JET AT x/d = 20.

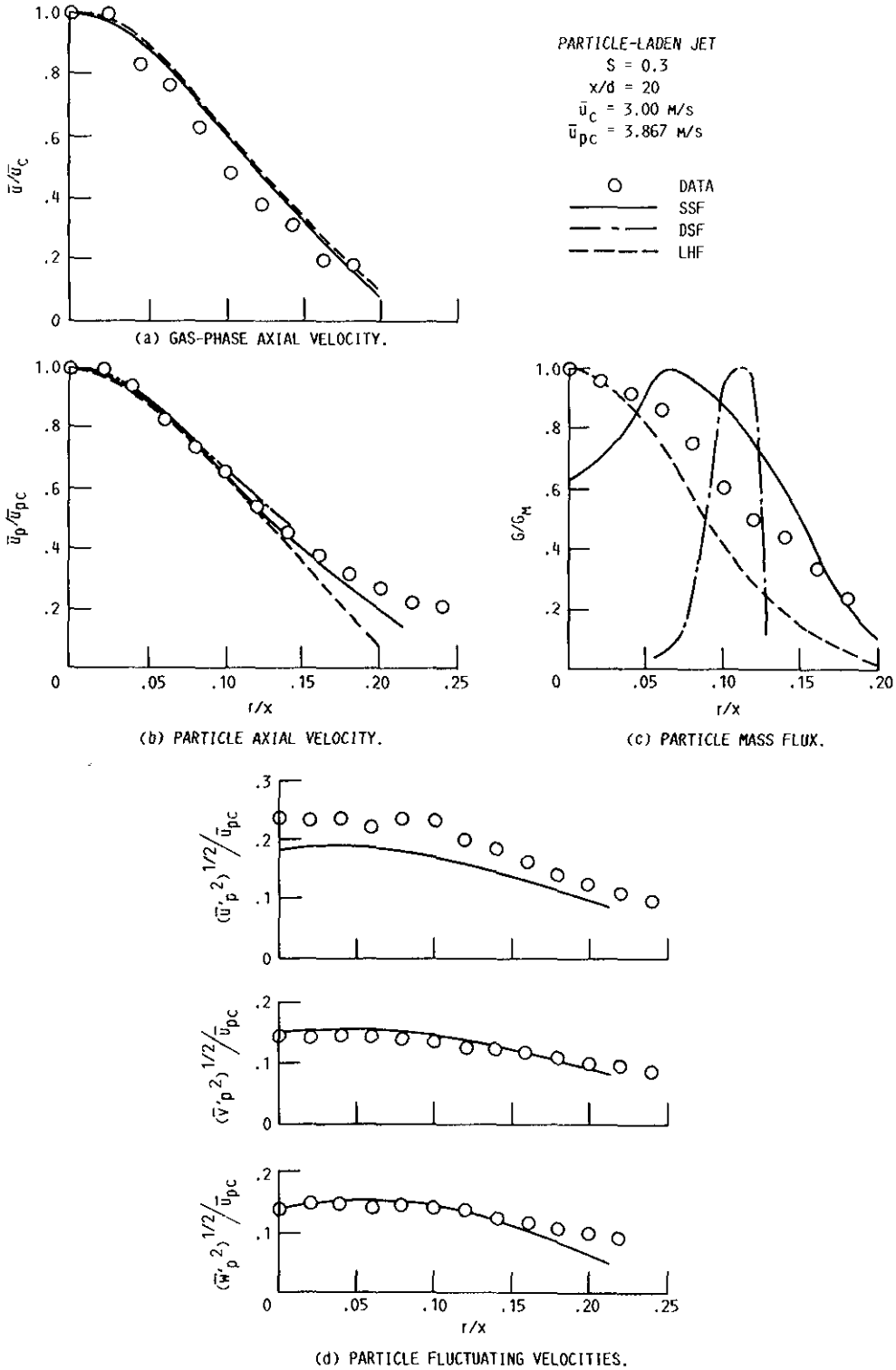

(a) GAS-PHASE AXIAL VELOCITY.

(b) PARTICLE AXIAL VELOCITY.

(c) PARTICLE MASS FLUX.

(d) PARTICLE FLUCTUATING VELOCITIES.

FIGURE 12. - RADIAL VARIATION OF NUMBER-AVERAGED FLOW PROPERTIES FOR THE SWIRLING (S = 0.3) PARTICLE-LADEN JET AT x/d = 20.

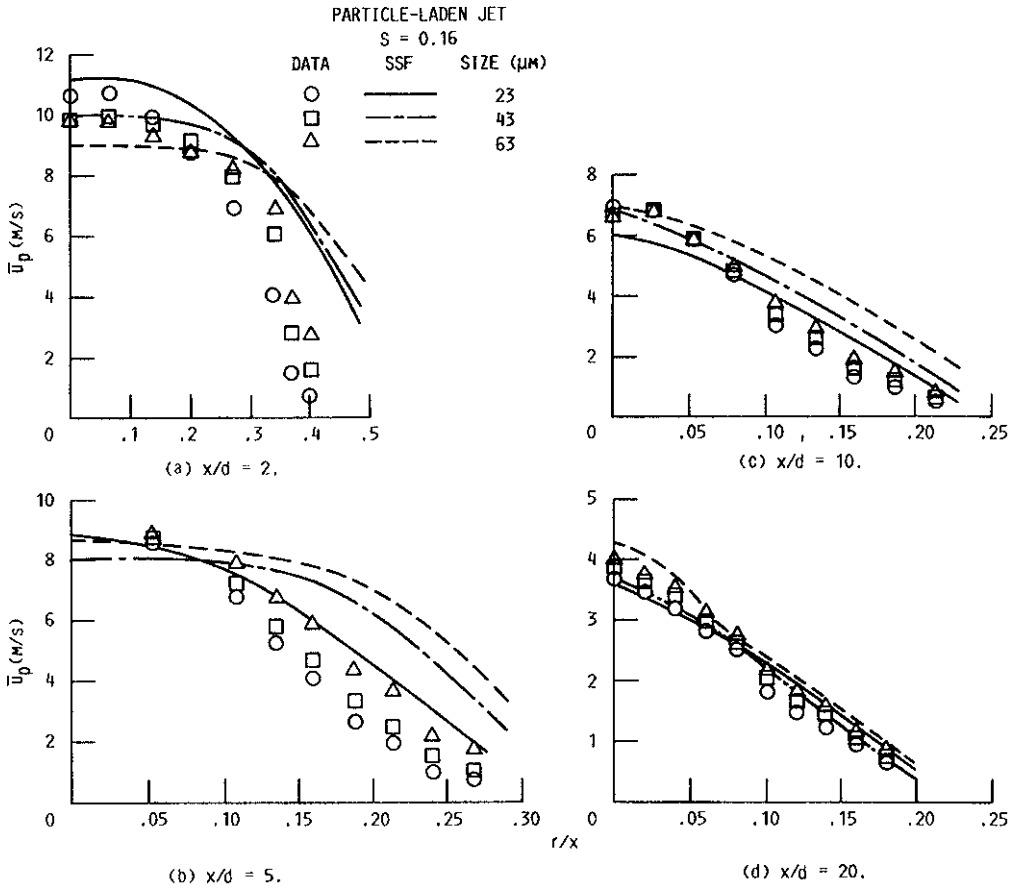

FIGURE 13. - RADIAL VARIATION OF MEAN AXIAL VELOCITY FOR 23, 43, AND 63 MICRON PARTICLES AT x/d = 2, 5, 10, AND 20 FOR THE PARTICLE-LADEN SWIRLING (S = 0.16) JET.

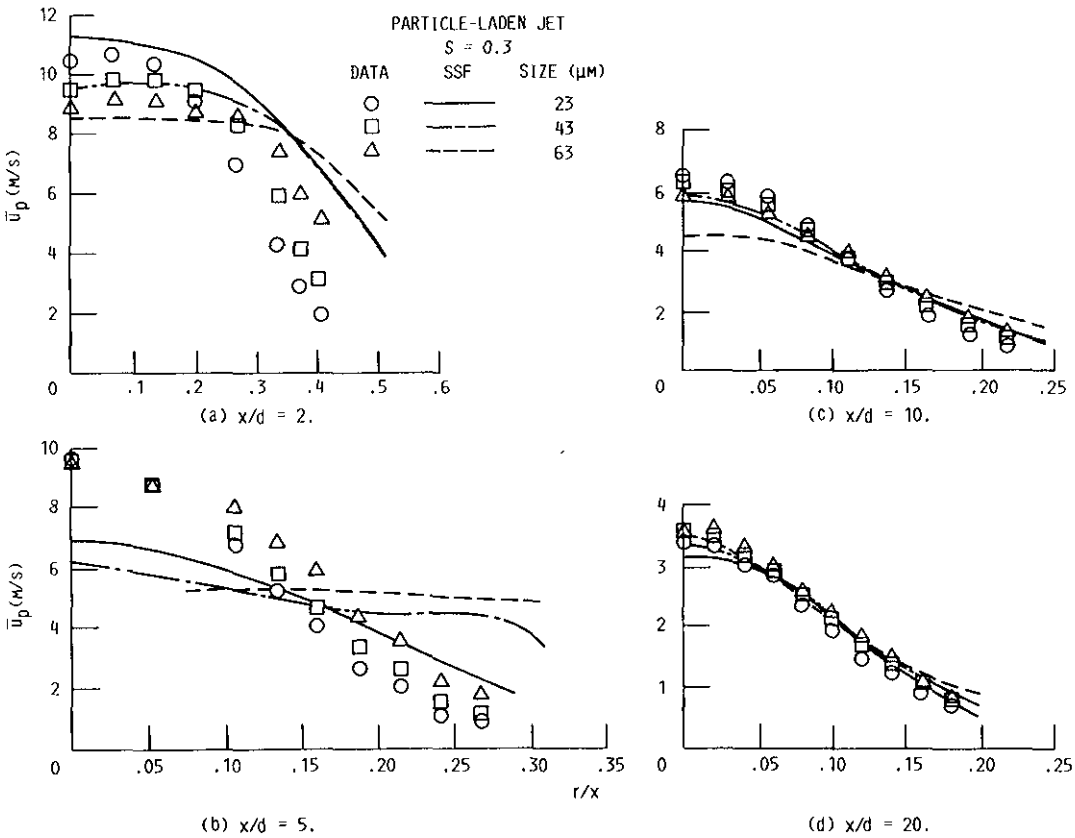

FIGURE 14. - RADIAL VARIATION OF MEAN AXIAL VELOCITY FOR 23, 43, AND 63 MICRON PARTICLES AT x/d = 2, 5, 10, AND 20 FOR THE PARTICLE-LADEN SWIRLING (S = 0.3) JET.

NASA
National Aeronautics and Space Administration

Report Documentation Page

1. Report No.	2. Government Accession No.	3. Recipient's Catalog No.
NASA TM-100920 AIAA-88-3138		

Title and Subtitle
Particle-Laden Weakly Swirling Free Jets: Measurements and Predictions

5. Report Date

6. Performing Organization Code
E-4176

7. Author(s)
Daniel L. Bulzan, Jian-Shun Shuen, and Gerard M. Faeth

8. Performing Organization Report No.
505-62-21

10. Work Unit No.

9. Performing Organization Name and Address
National Aeronautics and Space Administration
Lewis Research Center
Cleveland, Ohio 44135

11. Contract or Grant No.

13. Type of Report and Period Covered
Technical Memorandum

12. Sponsoring Agency Name and Address
National Aeronautics and Space Administration
Washington, D.C. 20546

14. Sponsoring Agency Code

15. Supplementary Notes
Prepared for the 24th Joint Propulsion Conference cosponsored by the AIAA, ASEE, ASME, and SAE, Boston, Massachusetts, July 11-13, 1988. Daniel L. Bulzan, NASA Lewis Research Center; Jian-Shun Shuen, Sverdrup Technology, Inc., (Lewis Research Center Group), NASA Lewis Research Center; Gerard M. Faeth, The University of Michigan, Ann Arbor, Michigan 48109.

16. Abstract

A theoretical and experimental investigation of particle-laden, weakly swirling, turbulent free jets was conducted. Glass particles, having a Sauter mean diameter of 39 μm with a standard deviation of 15 μm, were used in the study. A single loading ratio (the mass flow rate of particles per unit mass flow rate of air) of 0.2 was used in the experiments. Measurements are reported for three swirl numbers, ranging from 0 to 0.3. The measurements included mean and fluctuating velocities of both phases, and particle mass flux distributions. Measurements were compared with predictions from three types of multiphase flow analysis, as follows: (1) locally homogeneous flow (LHF), where slip between the phases was neglected; (2) deterministic separated flow (DSF), where slip was considered but effects of turbulence/particle interactions were neglected; and (3) stochastic separated flow (SSF), where effects of both interphase slip and turbulence/particle interactions were considered using random sampling for turbulence properties in conjunction with random-walk computations for particle motion. For the particle-laden jets, the LHF and DSF models did not provide very satisfactory predictions. The LHF model generally overestimated the rate of decay of particle mean axial and angular velocities with streamwise distance, due to the neglect of particle inertia. LHF model predictions of particle mass flux also showed poor agreement with measurements due to the assumption of no-slip between phases. The DSF model also performed quite poorly for predictions of particle mass flux, because turbulent dispersion of the particles was neglected. The SSF model, which accounts for both particle inertia and turbulent dispersion of the particles, yielded reasonably good predictions throughout the flow field for the particle-laden jets.

17. Key Words (Suggested by Author(s))	18. Distribution Statement
Particle-laden flows Swirling jets	Unclassified - Unlimited Subject Category 07

19. Security Classif. (of this report)	20. Security Classif. (of this page)	21. No of pages	22. Price*
Unclassified	Unclassified	22	A02

NASA FORM 1626 OCT 86

*For sale by the National Technical Information Service, Springfield, Virginia 22161